ADVANCED FUNCTIONAL MATERIALS
www.afm-journal.de

Electron Barrier Formation at the Organic-Back Contact Interface is the First Step in Thermal Degradation of Polymer Solar Cells

*I. T. Sachs-Quintana, Thomas Heumüller, William R. Mateker, Darian E. Orozco, Rongrong Cheacharoen, Sean Sweetnam, Christoph J. Brabec, and Michael D. McGehee**

Long-term stability of polymer solar cells is determined by many factors, one of which is thermal stability. Although many thermal stability studies occur far beyond the operating temperature of a solar cell which is almost always less than 65 °C, thermal degradation is studied at temperatures that the solar cell would encounter in real-world operating conditions. At these temperatures, movement of the polymer and fullerenes, along with adhesion of the polymer to the back contact, creates a barrier for electron extraction. The polymer barrier can be removed and the performance can be restored by peeling off the electrode and depositing a new one. X-ray photoelectron spectroscopy measurements reveal a larger amount of polymer adhered to electrodes peeled from aged devices than electrodes peeled from fresh devices. The degradation caused by hole-transporting polymer adhering to the electrode can be suppressed by using an inverted device where instead of electrons, holes are extracted at the back metal electrode. The problem can be ultimately eliminated by choosing a polymer with a high glass transition temperature.

1. Introduction

As the power conversion efficiency (PCE) of solution-processable, organic photovoltaics (OPVs) exceeds 10%,[1,2] the question of long-term stability becomes the next barrier to commercialization.[3–5] The record lifetime for a polymer OPV device is 6.2 years and was observed in glass encapsulated devices based on the polymer-fullerene blend of PCDTBT and $PC_{70}BM$.[6,7] The new lifetime record approximately doubled the previous lifetime record that was observed in P3HT:$PC_{60}BM$ OPV devices.[6]

Degradation in encapsulated polymer solar cells cannot be attributed to any one mechanism;[8–12] but, the different mechanisms of degradation in polymer solar cells can be classified into three general categories. The first category is light-induced burn-in degradation. This degradation is characterized by an exponential drop of about 20% of the initial efficiency and most of it occurs in the first 200 hours. The burn-in is found to be caused by photo-induced traps and is independent of the electrodes and the amount of injected current.[13,14] Two theories that attempt to explain the degradation include cross-linking[15] and light-induced breaking of C–H bonds.[16] The second category of degradation is long term degradation which is characterized by a slow, linear degradation. Of all of the degradation categories, the least is known about long-term degradation. A third category is thermal burn-in and is characterized by an exponential drop in efficiency that stabilizes over time. The highest solar cell temperature that solar cells are exposed to for a significant amount of time under solar illumination is 65 °C; this is the standard temperature used for testing thermal degradation.[17] Thermal degradation appears to be related to the interface. For example, PBDTTPD-based solar cells with power conversion efficiencies (PCE) of 7.3% suffer from thermal degradation and the loss in performance was shown to be restored by peeling off and reapplying the electrode.[18] To maximize the long-term performance of solar cells, all three of the degradation categories need to be addressed. In this paper we generalize the cause and solution of thermal burn-in for several polymer-fullerene systems. We show that thermal burn-in is caused by a less than 4 nm layer of polymer adhering to the back contact, where the back contact refers to the contact that is applied after the polymer-fullerene bulk-heterojunction (BHJ) film is processed. The polymer adhesion occurs at the glass transition temperature (T_g) of the polymer-fullerene blend. If the T_g of the polymer-fullerene blend is higher than 65 °C then

I. T. Sachs-Quintana, W. R. Mateker, D. E. Orozco, R. Cheacheroen, S. Sweetnam, Prof. M. D. McGehee
Department of Materials Science and Engineering
Stanford University
Stanford, CA 94305, USA
E-mail: mmcgehee@stanford.edu
T. Heumüller, C. J. Brabec
Institute of Materials for Electronics and Energy Technology (I-MEET)
Friedrich-Alexander-University Erlangen-Nuremberg
Martensstrasse 7, 91058 Erlangen, Germany
C. J. Brabec
Bavarian Center for Applied Energy Research (ZAE Bayern)
Haberstrasse 2a
91058 Erlangen, Germany

DOI: 10.1002/adfm.201304166

there is no thermal degradation under operating conditions. Using an inverted device also improves thermal stability. In an inverted device, holes are collected at the back contact, and inverted device performance is not affected by hole-conducting polymer adhering to the back contact. By using an inverted device geometry, the change in the vertical composition profile (VCP) does not form a barrier to charge collection.

While the effect of VCP of the polymer and the fullerene on initial performance has been observed by many research groups, this manuscript looks at how the VCP changes as the solar cell is annealed under typical solar cell operating temperatures of 65 °C. Campoy-Quiles et al. showed through ellipsometry experiments that a P3HT-PC_{60}BM blend changes its composition profile as it ages at 140 °C.[19] Yang et al. built on this work by measuring the VCP with X-ray photoelectron spectroscopy (XPS) prior to applying electrodes.[20] Both Yang and Campoy-Quiles observed that a skin layer of P3HT exists when the P3HT-PC_{60}BM blend is cast onto the substrate and that the skin layer of polymer is largely removed when the bulk heterojunction is annealed above the glass transition temperature. The P3HT skin layer at the top of the solar cell is detrimental to standard architecture devices because the polymer transports the holes and in a standard device, the back electrode is the electron-collecting contact. Yang et al. showed that the hole-transporting, P3HT skin layer next to the hole-collecting back contact can slightly improve the efficiency of inverted devices. Germack, DeLongchamp et al. confirmed the existence of the skin layer on bulk heterojunctions with ellipsometry.[21] By using a Nafion electron transport layer, they were able to decrease the amount of polymer present at the skin layer. Additional studies have observed the skin layer to exist on top of BHJs.[22,23] Using ellipsometry to find the composition gradient between two organics is difficult because the materials have similar electron density. Moulé's studies using neutron reflectivity (NR) circumvents this issue because the polymer and the fullerene have different neutron scattering length densities.[24] This manuscript adds to this literature by not just looking at initial efficiency but particularly by observing how vertical phase segregation that is not present in the fresh device, forms as the solar cell is aged over time at a normal solar cell operating temperature of 65 °C. We find that the degradation occurs within 4 nm of the BHJ-back contact interface. It is challenging to characterize this buried interface with sufficient resolution especially if there is any roughness. This challenge could cause the large variance in the reported amount of PCBM at the BHJ-back contact interface which range from 61% using NEXAFS to 91% using neutron reflectivity.[24] Rather than stretch the resolution limits of direct characterization techniques, we chose to systematically vary the electrodes and age devices to find that electron barrier formation at that interface is the first step in thermal degradation of polymer solar cells.

2. Results and Discussion

2.1. Thermal Degradation Begins at T_g

To determine the lowest temperature that causes degradation, we subjected the solar cells to a temperature step profile where we monitor the performance of solar cells for three hours at a time before increasing the temperature by 10 °C. The devices used in this temperature stepping study are optimized for efficiency. For all of the P3HT-based solar cells, the photoactive layer is annealed at 110 °C for 10 min prior to applying the electrodes, so the P3HT-based solar cells should not have a polymer skin layer.[19–21,24] The P3HT:PC_{60}BM BHJ was cast from o-dichlorobenzene on to a PEDOT:PSS/ITO substrate. The typical starting PCE for our P3HT:PC_{60}BM solar cells with Ca/Al electrodes was between 3.8 and 4.0%. The PCDTBT:PC_{70}BM solar cells are not annealed prior to depositing the electrode because annealing these solar cells above their glass transition temperature, 136 °C, is known to decrease the efficiency due to the formation of shallow traps and annealing is not necessary to obtain high-efficiency PCDTBT devices.[25] The PCDTBT:PC_{70}BM BHJ was cast from o-dicholorbenzene onto an PEDOT:PSS/ITO substrate. The starting PCE for these cells before aging was between 5.5 and 6.0%.

We found that thermal degradation begins near the T_g of the thin-film blend. **Figure 1**a shows that the open-circuit voltage (Voc) for P3HT:PC_{60}BM ceases to be flat with respect to time when the temperature is raised to 57 °C. This onset of degradation for P3HT:PC_{60}BM is close to the glass transition temperature of 56 °C for the polymer in the blend measured by DSC. The observed T_g corresponds to previous results.[26] Figure 1b shows that the Voc for PCDTBT:PC_{70}BM ceases to be flat with respect to time at 127 °C. From our DSC measurements the T_g for PCDTBT in the PCDTBT:PC_{70}BM blend is 136 °C. This is also in good agreement with the previously reported T_g values of 130 °C in the bulk[27] and 125 °C in the thin film.[28] Based on the measurements of the glass transition for PCDTBT in the polymer-fullerene bulk heterojunction (BHJ), it is not surprising that PCDTBT solar cells are thermally stable at operating temperatures. The low lifetime in the light that is observed for P3HT:PC_{60}BM compared to PCDTBT:PC_{70}BM in photostability tests is partly due to thermal degradation because the T_g of P3HT:PC_{60}BM is close to the temperature that the cells experienced under the sulfur-plasma lamp used in the lifetime test.[6]

The observed bulk glass-transition temperature of the neat polymer is often higher than the glass-transition temperature of the polymer that is observed in thin-films by as much as 10 °C.[29] The depression in T_g for thin films is attributed to the formation of a liquid-like layer of high polymer mobility at the surface.[30,31] The difference in T_g between the bulk and the thin-film is important to consider when testing a polymer's thermal stability.

2.2. A Proposed Model for Thermal Degradation

We suggest that degradation near the T_g of the solar cell is caused by a less than 4 nm thick layer at the interface of the BHJ and the back contact. We refer to the contact evaporated onto the BHJ that caps the solar cell as the back contact. This mechanism is consistent with previous work on thin polystyrene films where the polymer at the top of the film is more mobile.[32,33] The high polymer mobility at the top of these films was shown to be independant of the capping electrode.[34] After the solar cell has degraded, most of the performance can be restored

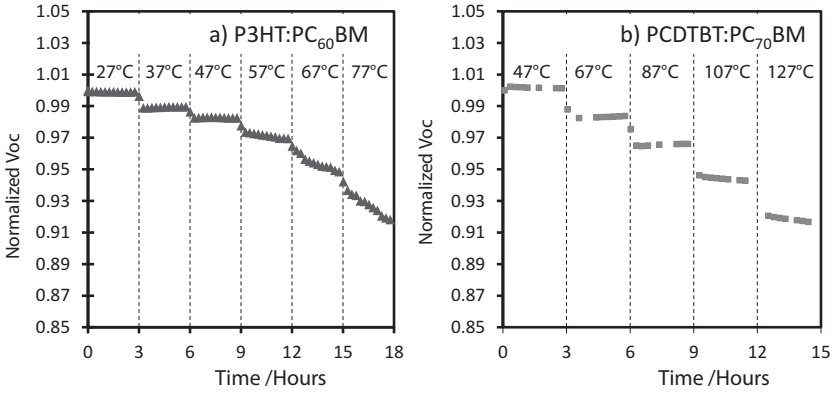

Figure 1. a) The normalized voltage loss for P3HT:$PC_{60}BM$ blends as a function of time and temperature. Device degradation is evident by a loss in voltage as a function of time and begins at 57 °C. b) Normalized voltage loss for PCDTBT:$PC_{70}BM$ blends as a function of time and temperature. A loss in voltage as a function of time appears to begin at 127 °C.

by peeling off and replacing the back contact. When the back contact is peeled off, the performance is restored in standard architacture devices because the hole-conducting polymer that was adhered to the top electron-collecting electrode is removed, thereby removing the barrier to electron collection.

Changing the back contact in devices dramatically changes the degradation rate. In an inverted architecture device, the hole-collecting contact is the back contact. A layer of hole-conducting polymer at the interface of the BHJ and the back contact would not hurt the performance, and in fact we find that the thermal degradation is suppressed for these devices. Furthermore, to show that the polymer adheres to the back contact and not to any specific material, we tested standard and inverted devices where PEIE and MoO_3 are used as the transport layers. The ITO/PEIE/P3HT:$PC_{60}BM$/MoO_3/Ag inverted devices show a supressed burn-in while the ITO/MoO_3/P3HT:$PC_{60}BM$/PEIE/Ag standard architecture devices degrade. This demonstrates that the polymer adhesion is not limited to polymer-metal interactions, but further suggests that a thin polymer layer is in fact forming at the back contact and can occur with any material.

We further ruled out degradation effects related to the bulk, the fullerene, and to the front contact. Photoluminescence quenching efficiency did not change during aging, which implies that the domain size for the polymer did not significantly change.[35] Varying the front contact did not change the thermal degradation behavior near T_g. We also demonstrate that fullerenes do not tend to adhere to the back electrode. Although it has been shown that fullerenes diffuse faster in a BHJ than the polymer,[36,37] evaporating a layer of pure C_{60} between the BHJ and the back contact did not prevent thermal burn-in implying that polymer adhered to the electrode by displacing the C_{60}. This observation strongly suggests that the polymer-back contact interface energy is higher than the interface energy between the polymer and the fullerene.

2.3. Replacing the Back Electrode Restores Device Performance

For both P3HT:$PC_{60}BM$ and PCDTBT:$PC_{70}BM$, thermal degradation appears to be related to the interface between the BHJ and the back contact because removing and replacing the back contact restores the majority of the efficiency lost to thermal degradation. **Figure 2** shows the *I–V* curves for the fresh (black squares) and thermally aged (blue circles) P3HT:$PC_{60}BM$ solar cells. The red curve with triangular markers in Figure 2 represents the device where the electrode from the aged cell was removed and reapplied. The electrode was mechanically delaminated by placing Kapton tape on top of the solar cell and peeling off the tape and the electrode.[18,38] **Table 1** shows the photovoltaic figures of merit for the solar cells in Figure 2. The power conversion efficiency (PCE) for the solar cell decreased from 3.8% to 2.2%. After the electrode is reapplied, the PCE is restored to 3.6%, thereby reversing 88% of the thermal degradation. Reapplying and restoring the electrode also recovered the degradation for devices that use higher adduct fullerenes. We observe that during thermal aging, the efficiency for P3HT:ICBA solar cells decreased from 5.4% to 4.5%. After the metal electrode is removed and reapplied, the efficiency was restored to 4.9%.

X-ray photoelectron spectroscopy (XPS) of the buried interface between the metal and photoactive layers shows that as the solar cell thermally degrades, more polymer-containing material adheres to the back contact. This buried interface was investigated by peeling off the Ca/Al electrode with Kapton tape and performing XPS on both the underside of the peel and on the top of the substrate. **Figure 3** and Figure S1 (Supporting Information) show the XPS spectra of the underside of the peel for P3HT:$PC_{60}BM$ and P3HT:ICBA devices, respectively. In XPS the weight or molar ratio of two elements can be estimated from their respective peak areas. We observed a higher S to Ca peak area ratio in the aged device compared to the fresh device, which implies that as the solar cell ages, more P3HT-containing organic material adheres to the electrode. We cannot

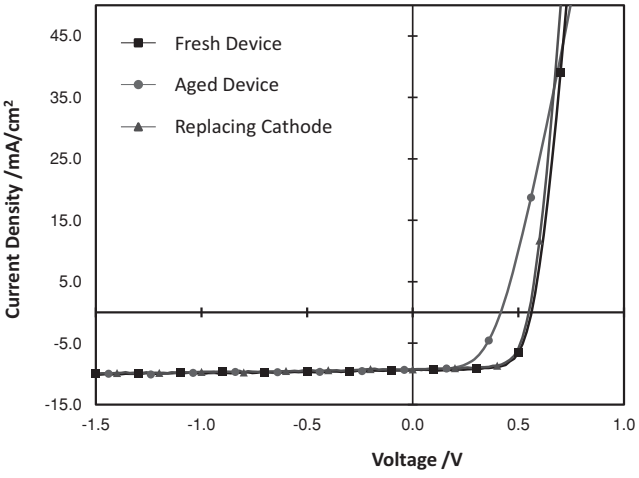

Figure 2. a) Illuminated *J–V* curves for a single P3HT:$PC_{60}BM$ solar cell aged for 50 h at 65 °C. Replacing the cathode of an aged device with a fresh electrode is shown to improve the voltage and the fill factor (FF).

Table 1. Figures of merit for a P3HT:$PC_{60}BM$ solar cell that was aged in the dark at 65 °C. Replacing the cathode of an aged device restores most of the performance.

Aging Condition [h]	J_{sc} [mA cm^{-2}]	V_{oc} [V]	FF	PCE [%]
0	9.4	0.56	0.71	3.8
50	9.3	0.42	0.58	2.2
new electrode	9.3	0.55	0.70	3.6

determine if the organic layer that adheres to the electrode over time is pure P3HT due to complications in the peel-off technique outlined in the Supporting Information. The fact that the organic layer increases in thickness suggests that a morphology change occurs at the interface between the back-contact and the BHJ. The XPS data and the device data could be explained by a layer of pure P3HT adhering to the back contact which would create an electron barrier and decrease device performance for standard architecture devices.

Ca photoelectrons are collected in all of the samples shown in Figure 3 and Figure S1 (Supporting Information), meaning that the P3HT-containing layer is thin enough that photoelectrons generated in Ca can reach the detector. The photoelectrons in the thin layer can reach the detector if they are generated within a depth of $3\lambda_{IMFP}\cos\theta$ from the top surface of a sample where λ_{IMFP} is the inelastic mean free path of electrons and θ is the angle between the spectrometer and the sample (45°). The inelastic mean free path of photoelectrons travelling in Ca or S is inferred to be 2 nm from several books and we calculate that the thickness of the P3HT-containing organic layer that is adhered to the Ca is no greater than 4 nm.[39–41] Where a material delaminates depends on many factors[42,43] and it is difficult to calculate the exact thickness and the blend ratio of P3HT and PCBM on the peeled electrode for reasons outlined in the Supporting Information; however, when coupled with studies on working solar cells with different electrodes, the increase in the S to Ca ratio over time strongly suggests that an electron-blocking pure P3HT layer is adhering to the back contact as the solar cell is aged at 65 °C.

2.4. Inverted Devices are Inherently More Thermally Stable

Changing the back electrode changed the severity of thermal degradation at 65 °C for P3HT:$PC_{60}BM$ solar cells. **Figure 4**a shows that the Ca/Al electrode is the most stable low work function electrode and that bare Al is the least stable low work function electrode, in agreement with the previous findings of Reese et al.[44] Further, we show that inverted devices did not lose efficiency on the same time scale as the standard architecture devices and actually improved slightly over time (Figure 4a).

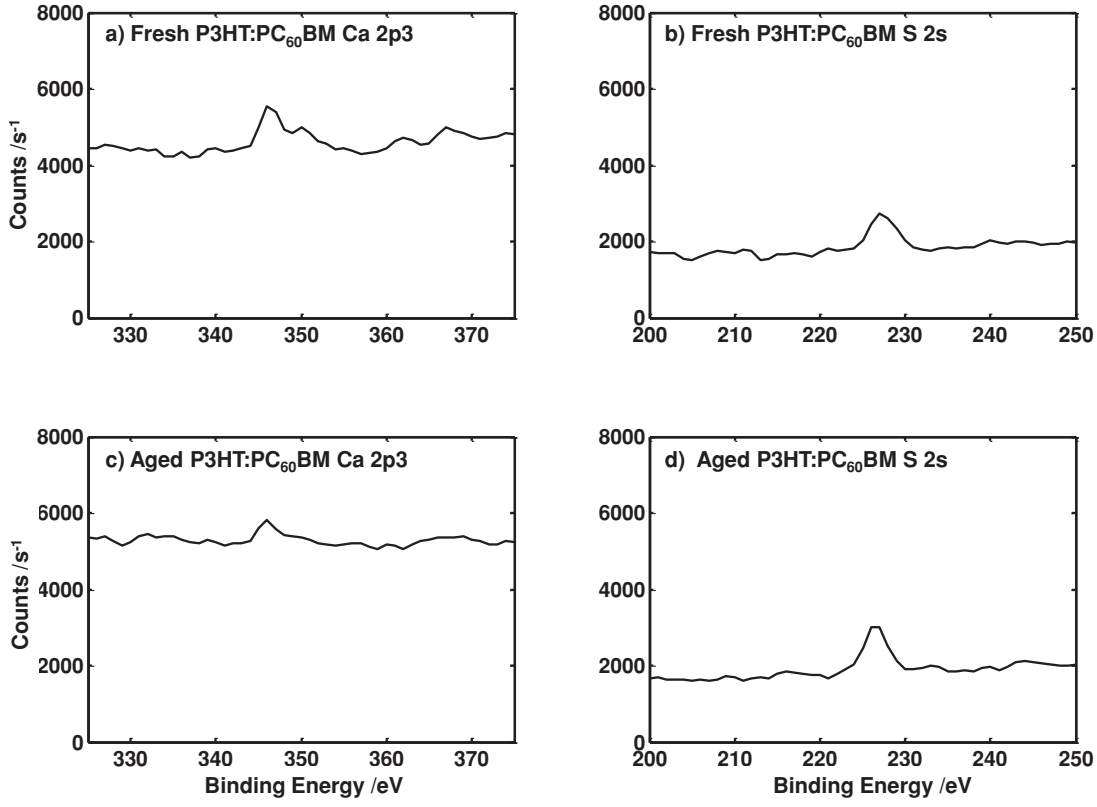

Figure 3. a) XPS Ca peak and b) S peak on the underside of the peeled electrode from a P3HT:$PC_{60}BM$ device. c) XPS Ca peak and d) S peak on the underside of the peeled electrode from a P3HT:$PC_{60}BM$ device that has been aged at 65°C. The S/Ca peak area ratio is related to how much P3HT remains on the electrode.

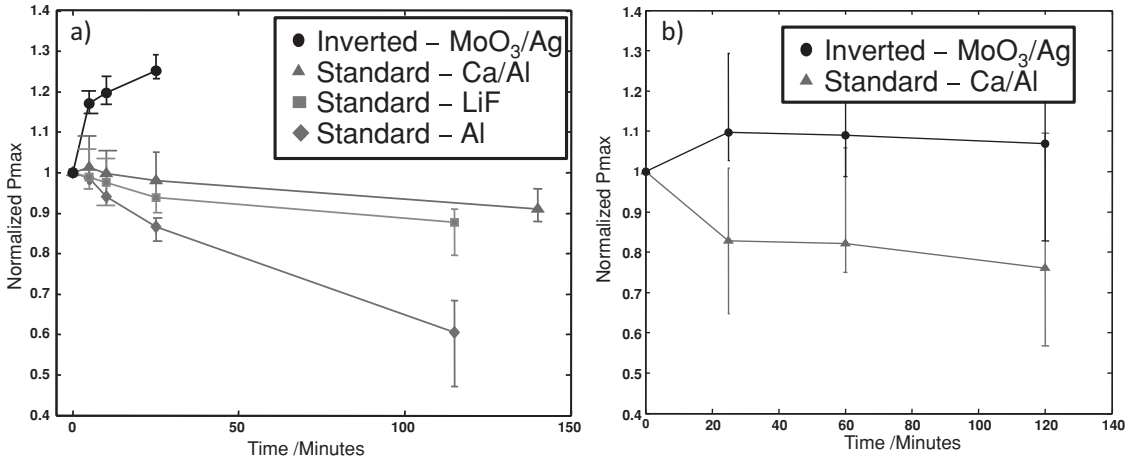

Figure 4. a) Degradation of P3HT:$PC_{60}BM$ and b) PCDTBT:$PC_{70}BM$ devices with different back contacts. The bottom contact for the standard devices is PEDOT:PSS; for the inverted devices the bottom contact is PEIE. The error-bars represent the spread in degradation for 10 devices.

The inverted devices use a polyethylenimine ethoxylated (PEIE) interlayer as an electron transport material at the bottom contact and a MoO_3/Ag back contact.[45] Solar cells that use PCDTBT:$PC_{70}BM$ active layers were also more thermally stable in an inverted architecture than in the standard architecture, as shown in Figure 4b. The devices in Figure 4b are optimized; the top starting PCE is 6.2% for the standard device and 5.3% for the inverted device. Thermal degradation near T_g for the optimized PCDTBT solar cells showed a similar effect that was observed for P3HT-based solar cells because the inverted devices improved slightly in efficiency while the standard architecture devices degraded. In this experiment, two aspects of the solar cell were changed: the metal-BHJ interface was removed and replaced with a MoO_3-BHJ interface, and an inverted architecture was used. Changing both makes it difficult to differentiate whether the increase in device stability is general to the inverted architecture or due to replacing the metal-organic interface.

To determine whether the improvement in stability is due to the inverted architecture or to removing the metal-organic interface, we compared standard and inverted devices utilizing the same electrodes. To rule out the possibility that degradation was due to particular chemical interactions between the BHJ and the electrode materials, and not more general to device architecture, the degradation of ITO/PEIE/P3HT:$PC_{60}BM$/MoO_3/Ag inverted devices were compared to the degradation of ITO/MoO_3/P3HT:$PC_{60}BM$/PEIE/Ag standard architecture devices. In this experiment, the materials used in the solar cell are the same, and only the order of the MoO_3 and the PEIE in the solar cell stack are switched. If an interaction between a specific material and the BHJ is occurring then both the standard and the inverted device should degrade. **Figure 5** shows that the standard devices degrade in the dark at 65 °C, while the inverted devices show a slight improvement, which is consistent with a model where the polymer adheres to the back contact. The adhesion at the BHJ-back contact interface appears to be insensitive to which back contact is used because standard architecture devices with LiF, Ca, or PEIE electron transport layers degrade.

To confirm that the polymer chains interact more strongly with the electrode and displaces the fullerene we made devices with a pure C_{60} layer inserted between the BHJ and the back contact. The C_{60} layer was used to physically block the polymer from adhering to the back contact; however, degradation still occurred showing that the fullerene does not adhere to the electrode (Figure S2, Supporting Information). When the solar cells were heated above the T_g both the polymer and the fullerene move, but only the polymer adheres to the top electrode. Fullerenes are known to diffuse rapidly through the BHJ,[36,37] but the fullerene does not have a large impact on thermal degradation near T_g because it does not adhere to the back contact. The thin polymer layer that adheres to the electrode is similar to the skin layer that is found in as-cast BHJs. The P3HT-based devices in this study were annealed at 110 °C for ten minutes prior to electrode deposition which is known to remove the skin layer present in as-cast devices.[19,20,24] Thermal degradation near T_g of the completed device causes a skin layer to reform and adhere to the back contact.

It is interesting that the polymer appears to displace fullerenes and adheres to the back contact electrode but it does not adhere to the front contact. We suggest that the skin layer forms

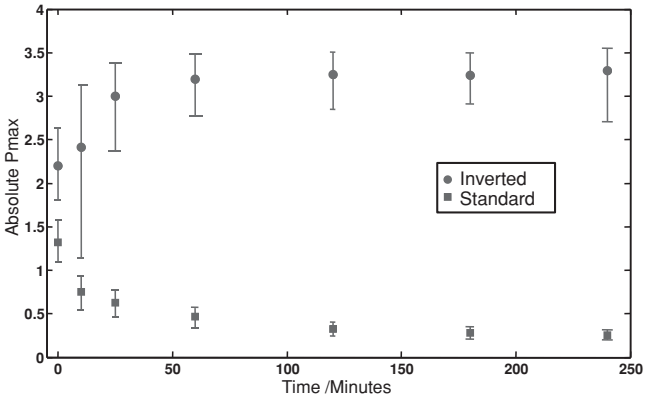

Figure 5. Degradation in the power conversion efficiency of ITO/PEIE/P3HT:$PC_{60}BM$/MoO_3/Ag inverted devices (circle) and ITO/MoO_3/P3HT:$PC_{60}BM$/PEIE/Ag standard architecture devices (square). In this test, the materials used in the solar cell are the same, only the order of the MoO_3 and the PEIE in the solar cell stack are switched.

during aging because the top of a thin polymer film is a region of higher polymer mobility. The mobility in thin polymer films is often described by a "three layer model", a top layer at the with a low T_g, a middle layer with a T_g equal to that of the bulk, and an immobile or "dead" layer that is adhered to the substrate.[32–34] The "dead" layer is needed to successfully model capacitance and positron annihilation data of thin polystyrene films on metal.[32,34] To physically demonstrate the inertness of the dead layer, Nguyen et al. annealed a thin film of polystyrene on Al and rinsed it in a good solvent. Although most of the thin film was dissolved, an irreversibly adsorbed layer of 8 nm remained. In contrast to the "dead layer," the layer of polymer that is on the top of the polymer thin film is highly mobile and has a lower glass transition temperature than the rest of the thin-film. Fukao found that the high mobility at the top of the thin film is independent of the capping electrode.[34] This high mobility layer of hole-transporting polymer adhering to the back, metal cathode acts as a barrier for electron extraction and would be consistent with the observed loss in Voc and FF. These barriers are well-known to cause a loss in fill factor[46–49] and voltage.[50,51] Polymer moving and adhering to the back electrode is consistent with our observation that the majority of the performance in standard architecture devices can be restored by removing and reapplying the electrode.

2.5. Thermal Degradation Near T_g is not Affected by the Bottom Contact, Thermal History, or the Bulk

Additional experiments demonstrate that the observed short-term thermal degradation near T_g occurs primarily at the back, and not the front electrode. Figure S3 shows that the degradation for a P3HT:PC_{60}BM device aged in the dark at 65 °C is similar for PEDOT:PSS, MoO_3, and V_2O_5 bottom contacts. This observation is consistent with the three-layer model of thin polymer films near T_g where the polymer near the substrate is relatively immobile and has a higher T_g than the rest of the film. Additionally, P3HT:PC_{60}BM films were spun on an ITO/PEDOT:PSS substrate and "pre-aged" for three days prior to applying the back contact at 65 °C. Upon applying the electrode, the efficiency was 4.0% for the devices that were pre-aged and 4.1% for the control devices that were not pre-aged. The observation that neither the choice of bottom electrode nor pre-aging the device hurts the solar cell performance implies that the front contact does not contribute to thermal degradation at the temperature where solar cells are operated. It also implies that degradation only occurs after the back contact has been deposited.

The role of thermal history was observed by testing solar cells that were post-annealed after the electrical contacts were applied. To make the post-annealed cells, the BHJ was cast onto an ITO/PEDOT:PSS substrate. Then, the electrodes were deposited after the BHJ was dried. After the electrodes were applied, the solar cells were post-annealed at 110 °C for ten minutes. After the cells are annealed, the solar cell efficiency was measured and the devices were aged at 65 °C. We see in Figure S4 that the efficiency of both post-annealed and pre-annealed devices decrease during aging at 65 °C. This occurs if the casting solvent is dichlorobenzene or chlorobenzene. The results of this study imply that at a typical operating temperature of a solar cell like 65 °C, the polymer can adhere to the back-contact independent of the starting morphology.

The short-term degradation that we observe near T_g does not appear to occur in the bulk of the film. The photoluminescence, a measure of the effectiveness of exciton splitting,[35] does not significantly change: after one hour of aging at 65 °C, the photoluminescence quenching efficiency of P3HT:PC_{60}BM changed from 93.8% ± 2% to 94.0% ± 2%. Although phase segregation and the accompanying increase in photoluminescence in OPV devices is observed by other research groups, this often occurs at temperatures much higher than the operating temperature of the solar cell.[52,53] The lack of a significant change in the photoluminescence spectra is consistent with the device data because there is no significant change in the current of the solar cells as seen in Table 1. The voltage can also be affected by phase segregation by decreasing the interfacial area between the polymer and fullerene, thereby decreasing the external quantum efficiency (EQE) of the charge transfer state.[54] It has been shown for MDMO-PPV:PC_{60}BM solar cells that the charge transfer state EQE decreases and red-shifts when the polymer is heated at 110 °C.[55] Figure S5 (Supporting Information) shows that the charge-transfer-state EQE for a P3HT:PC_{60}BM and P3HT:ICBA solar cell does not change when the solar cell is aged at 65 °C.

Thermal degradation is largely independent of the fullerene as shown in Figure S6 (Supporting Information). The thermal degradation rate at 65 °C for P3HT:PC_{60}BM and P3HT:ICBA cells were compared and the degradation behavior was qualitatively similar. PCDTBT:PC_{70}BM and PCDTBT:PC_{60}BM cells were also aged in parallel at 125 °C near the T_g of PCDTBT and the difference in degradation characteristics was much smaller than that resulting from changes in the architecture or the polymer. Synchrotron X-ray radiation can be used to observe morphological changes in the photoactive layer.[56,57] No change in the morphology was observed in grazing incidence X-ray diffraction experiments. These results imply that the majority of the short-term, thermal degradation is limited to the top interface and not related to the bulk of the material.

3. Conclusions

We demonstrated that for multiple systems, thermal degradation near the glass transition temperature of the solar cell is related to the interface between the back contact and the BHJ. Thermal degradation in standard architecture devices is caused by a thin polymer layer forming at the back contact and creating an electron blocking layer between the BHJ and the electron extracting electrode. In an inverted device, the back contact collects the holes, and having a thick layer of hole-transporting polymer next to the hole-collecting back contact is not harmful for inverted devices. Thermal degradation at operating temperatures can be eliminated by choosing a polymer that has a T_g in the BHJ thin film of greater than 65 °C, such as PCDTBT. To isolate the effects of burn-in caused by photochemical reactions from thermal burn-in, researchers should heat their cells for several hours at the temperature that the cells reach under the lamp before light soaking. This method will make it possible to study one type of degradation at a time. Although this manu-

script characterized and suggests solutions to thermal degradation for polymer solar cells at operating temperatures, further work is needed to understand and eliminate photo-induced burn-in and long-term photodegradation.

4. Experimental Section

Device fabrication: Glass substrates patterned with ITO (15 Ω sq^{-1}, Xinyan Technologies LTD) were scrubbed with a Extran 300 detergent diluted with water in a 9:1 ratio, ultrasonicated in the dilute Extran 300 detergent for 10 min, rinsed in de-ionized (DI) water for 5 min, sequentially ultrasonicated in acetone and isopropyl alcohol baths for 15 min, and exposed to a UV-ozone plasma for 15 min. An aqueous solution of PEDOT:PSS (Clevios P VP AI 4083) was spin-cast at 4000 rpm for 35 s onto the substrates and baked at 140 °C for 10 min. Substrates were next transferred into a dry nitrogen glovebox (<5 ppm O_2). P3HT was used as received (BASF P200). $PC_{60}BM$ and $PC_{70}BM$ was used as received and purchased from Solenne BV. ICBA was used as received from Plextronics. PCDTBT was used as received from St. Jean Photochemie. P3HT and PCDTBT solutions used dichlorobenzene as a solvent and were prepared in the glovebox. Active layers were spin-cast at 75 °C. Optimized P3HT solar cells used 25 mg P3HT mL^{-1} and 25 mg $PC_{60}BM$ mL^{-1} and were spun cast at 900 rpm for 45 s. The solution concentration and the spin speed were the same for P3HT:ICBA solar cells. The P3HT:$PC_{60}BM$ devices and the P3HT:ICBA were annealed at 110 °C prior to electrode deposition. Optimized PCDTBT solar cells used 4 mg PCDTBT ml^{-1} and 16 mg $PC_{70}BM$ mL^{-1} Electrodes were thermally evaporated at ≈ 10^{-6} Torr. Ca/Al electrodes consisted of a 7 nm Ca layer and a 150 nm Al layer. LiF/Al electrodes used 1 nm of LiF and 150 nm of Al. MoO_3/Ag devices had 10 nm of MoO_3 and 150 nm of Ag. For inverted devices, a PEIE (Sigma-Aldrich) was used as an electron transport material. PEIE was dissolved in 2-methoxyethanol at a concentration of 0.4 wt% PEIE. The 2-methoxyethanol/PEIE solution was spun at 5000 rpm for one minute in a laminar flow hood outside of the glovebox. After spinning the PEIE solution, the substrate was rinsed in DI water. To make standard architecture devices with PEIE, the PEIE was applied in the laminar flow hood after the P3HT:$PC_{60}BM$ layer was dry. The C_{60} (Sigma-Aldrich, sublimed) interlayers were thermally evaporated to a thickness of 10 nm.

Device Characterization: *J–V* measurements were performed in the glovebox using a Keithley 2400 source meter and a Spectra-Physics 91160–1000 solar simulator (calibrated to 1 sun, AM1.5 G, with a NREL certified KG-5 filtered silicon photodiode). Sub-band gap EQE was measured by exposing the solar cell to light from a monochrometer. The electrical signal from the solar cell first went through a transimpedence amplifier to minimize instrumentation shunt resistance and then the voltage signal was ultimately recorded with a Stanford Research Systems SR830 DSP lock-in amplifier. The chopping frequency of the probe beam used in the EQE experiments was 200 Hz.

Thermal Aging: Thermal degradation was executed at 65 °C in the dark in a nitrogen-filled glovebox with an oxygen partial pressure of less than 4x 10^{-4} Torr for the data presented in Figures 2–4, and Supporting Information Figures S1,S3–S5. For the remaining figures, thermal degradation was executed at 65 °C in a cryostat at vacuum with an oxygen partial pressure of approximately 10^{-6} Torr.

Photoluminescence (PL): Ten spectra were collected per device for each point during the aging experiment. An Ar-ion laser (λ = 514 nm) was used to illuminate the sample in a nitrogen-filled chamber and PL was measured with a Princeton Instruments spectrophotometer with a silicon CCD detector that was corrected for the instrument response. PL quenching was determined by dividing the PL of the solar cell by the PL of a pure, P3HT sample. To correct for differences is absorption, the PL quenching was multiplied by the ratio of the P3HT sample absorption at 514 nm to the solar cell absorption at 514 nm.

XPS: X-ray photoelectron spectroscopy was performed using a PHI 5000 VersaProbe with a Al K-alpha X-ray source. Data was collected at a vacuum of approximately 5 × 10^{-10} Torr with a probe angle 45° to the substrate. Electrodes were peeled by gently adhering the Kapton tape to the solar cell and peeling the electrode off by hand.

DSC: DSC was performed using a TA Instruments Q2000 differential scanning calorimeter at a nitrogen flow of 50 mL min^{-1}. Samples were fabricated by drop casting the photovoltaic blend solution mentioned in the device fabrication section. After the sample was dry, it was scraped into a Tzero hermetically sealed pan. At least 5 mg of material was used to determine T_g. The samples were allowed to equilibrate at room temperature before ramping at a rate of 10 °C min^{-1} to 300 °C.

GIXD: PEDOT:PSS and the active layers were spin-cast onto cleaned silicon substrates using the procedures outlined previously. GIXD experiments were carried out at the Stanford Synchrotron Radiation Lightsource beamline 11–3 using photon energy of 12.7 keV, a MAR345 image plate area detector, a helium-filled sample chamber, and an incident X-ray beam angle of ≈0.12°.

Supporting Information

Supporting Information is available from the Wiley Online Library or from the author.

Acknowledgements

The authors would like to acknowledge Koen Vandewal, and Chuck Hitzman for sharing their expertise on sub-bandgap EQE, and XPS, respectively. The authors would also like to thank Christine McGuiness at Plextronics for supplying ICBA and for her helpful discussions. TH gratefully acknowledges the "DAAD Doktorantenstipedium" and the SFB 953 "Synthetic Carbon Allotropes" This publication was based on work supported by the Center for Advanced Molecular Photovoltaics (CAMP) (Award No KUS-C1–015–21), made by King Abdullah University of Science and Technology (KAUST).

Received: December 13, 2013
Revised: January 17, 2014
Published online: March 24, 2014

[1] M. A. Green, K. Emery, Y. Hishikawa, W. Warta, E. D. Dunlop, *Prog. Photovoltaics Res. Appl.* **2013**, *21*, 827.
[2] J. You, L. Dou, K. Yoshimura, T. Kato, K. Ohya, T. Moriarty, K. Emery, C.-C. Chen, J. Gao, G. Li, Y. Yang, *Nat. Commun.* **2013**, *4*, 1.
[3] M. Jørgensen, K. Norrman, S. A. Gevorgyan, T. Tromholt, B. Andreasen, F. C. Krebs, *Adv. Mater.* **2012**, *24*, 580.
[4] C. J. Brabec, S. Gowrisanker, J. J. M. Halls, D. Laird, S. Jia, S. P. Williams, *Adv. Mater.* **2010**, *22*, 3839.
[5] B. Azzopardi, C. J. M. Emmott, A. Urbina, F. C. Krebs, J. Mutale, J. Nelson, *Energy Environ. Sci.* **2011**, *4*, 3741.
[6] C. H. Peters, I. T. Sachs-Quintana, J. P. Kastrop, S. Beaupré, M. Leclerc, M. D. McGehee, *Adv. Energy Mater.* **2011**, *1*, 491.
[7] R. Roesch, K.-R. Eberhardt, S. Engmann, G. Gobsch, H. Hoppe, *Sol. Energy Mater. Sol. Cells* **2013**, *117*, 59.
[8] J. A. Hauch, P. Schilinsky, S. A. Choulis, S. Rajoelson, C. J. Brabec, *Appl. Phys. Lett.* **2008**, *93*, 103306.
[9] K. Norrman, M. V. Madsen, S. A. Gevorgyan, F. C. Krebs, *J. Am. Chem. Soc.* **2010**, *132*, 16883.
[10] A. Rivaton, A. Tournebize, J. Gaume, P.-O. Bussière, J.-L. Gardette, S. Therias, *Polym. Int.*, **2013**
[11] H. Hintz, H.-J. Egelhaaf, L. Lüer, J. Hauch, H. Peisert, T. Chassé, *Chem. Mater.* **2011**, *23*, 145.

[12] E. T. Hoke, I. T. Sachs-Quintana, M. T. Lloyd, I. Kauvar, W. R. Mateker, A. M. Nardes, C. H. Peters, N. Kopidakis, M. D. McGehee, *Adv. Energy Mater.* **2012**, *2*, 1351.
[13] C. H. Peters, I. T. Sachs-Quintana, W. R. Mateker, T. Heumueller, J. Rivnay, R. Noriega, Z. M. Beiley, E. T. Hoke, A. Salleo, M. D. McGehee, *Adv. Mater.* **2012**, *24*, 663.
[14] T. M. Clarke, C. Lungenschmied, J. Peet, N. Drolet, K. Sunahara, A. Furube, A. J. Mozer, *Adv. Energy Mater.* **2013**, *3*, 1473.
[15] A. Tournebize, P.-O. Bussiere, A. Rivaton, J.-L. Gardette, H. Medlej, R. C. Hiorns, C. Dagron-Lartigau, F. C. Krebs, K. Norrman, *Chem. Mater.* **2013**, *25*, 4522.
[16] R. A. Street, D. M. Davies, *Appl. Phys. Lett.* **2013**, *102*, 043305.
[17] M. O. Reese, S. A. Gevorgyan, M. Jørgensen, E. Bundgaard, S. R. Kurtz, D. S. Ginley, D. C. Olson, M. T. Lloyd, P. Morvillo, E. A. Katz, *Sol. Energy Mater. Sol. Cells* **2011**, *95*, 1253.
[18] W. R. Mateker, J. D. Douglas, C. Cabanetos, I. T. Sachs-Quintana, J. A. Bartelt, E. T. Hoke, A. El Labban, P. M. Beaujuge, J. M. J. Fréchet, M. D. McGehee, *Energy Environ. Sci.* **2013**, *6*, 2529.
[19] M. Campoy-Quiles, T. Ferenczi, T. Agostinelli, P. G. Etchegoin, Y. Kim, T. D. Anthopoulos, P. N. Stavrinou, D. D. C. Bradley, J. Nelson, *Nat. Mater.* **2008**, *7*, 158.
[20] Z. Xu, L.-M. Chen, G. Yang, C.-H. Huang, J. Hou, Y. Wu, G. Li, C.-S. Hsu, Y. Yang, *Adv. Funct. Mater.* **2009**, *19*, 1227.
[21] D. S. Germack, C. K. Chan, R. J. Kline, D. A. Fischer, D. J. Gundlach, M. F. Toney, L. J. Richter, D. M. DeLongchamp, *Macromolecules* **2010**, *43*, 3828.
[22] A. J. Parnell, A. D. F. Dunbar, A. J. Pearson, P. A. Staniec, A. J. C. Dennison, H. Hamamatsu, M. W. A. Skoda, D. G. Lidzey, R. A. L. Jones, *Adv. Mater.* **2010**, *22*, 2444.
[23] J. W. Kiel, B. J. Kirby, C. F. Majkrzak, B. B. Maranville, M. E. Mackay, *Soft Matter* **2010**, *6*, 641.
[24] S. A. Mauger, L. Chang, S. Friedrich, C. W. Rochester, D. M. Huang, P. Wang, A. J. Moulé, *Adv. Funct. Mater.* **2013**, *23*, 1935.
[25] Z. M. Beiley, E. T. Hoke, R. Noriega, J. Dacuña, G. F. Burkhard, J. A. Bartelt, A. Salleo, M. F. Toney, M. D. McGehee, *Adv. Energy Mater.* **2011**, *1*, 954.
[26] J. Zhao, A. Swinnen, G. Van Assche, J. Manca, D. Vanderzande, B. Van Mele, *J. Phys. Chem. B* **2009**, *113*, 1587.
[27] B. N. Blouin, A. Michaud, M. Leclerc, *Adv. Mater.* **2007**, *19*, 2295.
[28] T. Wang, A. J. Pearson, A. D. F. Dunbar, P. A. Staniec, D. C. Watters, H. Yi, A. J. Ryan, R. A. L. Jones, A. Iraqi, D. G. Lidzey, *Adv. Funct. Mater.* **2012**, *22*, 1399.
[29] H. K. Nguyen, M. Labardi, M. Lucchesi, P. Rolla, D. Prevosto, *Macromolecules* **2013**, *46*, 555.
[30] J. L. Keddie, R. A. L. Jones, R. A. Cory, *Europhys. Lett.* **1994**, *27*, 59.
[31] J. L. Keddie, R. A. L. Jones, R. A. Cory, *Faraday Discuss.* **1994**, *98*, 219.
[32] G. DeMaggio, W. Frieze, D. Gidley, M. Zhu, H. Hristov, A. Yee, *Phys. Rev. Lett.* **1997**, *78*, 1524.
[33] S. Napolitano, M. Wübbenhorst, *J. Phys. Chem. B* **2007**, *111*, 9197.
[34] K. Fukao, Y. Miyamoto, *Phys. Rev. E. Stat. Phys. Plasmas. Fluids. Relat. Interdiscip. Topics* **2000**, *61*, 1743.
[35] H. Hoppe, N. S. Sariciftci, *J. Mater. Chem.* **2006**, *16*, 45.
[36] N. D. Treat, M. A. Brady, G. Smith, M. F. Toney, E. J. Kramer, C. J. Hawker, M. L. Chabinyc, *Adv. Energy Mater.* **2011**, *1*, 82.
[37] D. Chen, F. Liu, C. Wang, A. Nakahara, T. P. Russell, *Nano Lett.* **2011**, 2071.
[38] Q. Wang, Y. Luo, H. Aziz, *Appl. Phys. Lett.* **2010**, *97*, 063309.
[39] P. van der Heide, *X-Ray Photoelectron Spectroscopy: An Introduction to Principles and Practices*, Wiley, Hoboken, NJ, USA **2012**.
[40] C. C. Chusuei, D. W. Goodman, *Encyclopedia of Physical Science and Technology: X-Ray Photoelectron Spectroscopy*, Academic Press, Waltham, MA, USA **2003**.
[41] P. J. Cumpson, M. P. Seah, *Surf. Interface Anal.* **1997**, *25*,1 430.
[42] S. R. Dupont, M. Oliver, F. C. Krebs, R. H. Dauskardt, *Sol. Energy Mater. Sol. Cells* **2012**, *97*, 171.
[43] V. Brand, C. Bruner, R. H. Dauskardt, *Sol. Energy Mater. Sol. Cells* **2012**, *99*, 182.
[44] M. O. Reese, M. S. White, G. Rumbles, D. S. Ginley, S. E. Shaheen, *Appl. Phys. Lett.* **2008**, *92*, 053307.
[45] Y. Zhou, C. Fuentes-Hernandez, J. Shim, J. Meyer, A. J. Giordano, H. Li, P. Winget, T. Papadopoulos, H. Cheun, J. Kim, M. Fenoll, A. Dindar, W. Haske, E. Najafabadi, T. M. Khan, H. Sojoudi, S. Barlow, S. Graham, J.-L. Brédas, S. R. Marder, A. Kahn, B. Kippelen, *Science* **2012**, *336*, 327.
[46] J. Wagner, M. Gruber, A. Wilke, Y. Tanaka, K. Topczak, A. Steindamm, U. Hörmann, A. Opitz, Y. Nakayama, H. Ishii, J. Pflaum, N. Koch, W. Brütting, *J. Appl. Phys.* **2012**, *111*, 054509.
[47] H. Jin, M. Tuomikoski, J. Hiltunen, A. Maaninen, F. Pino, *J. Phys. Chem. C* **2009**, *113* 16807.
[48] D. Gupta, S. Mukhopadhyay, K. S. Narayan, *Sol. Energy Mater. Sol. Cells* **2010**, *94*, 1309.
[49] D. Gupta, M. Bag, K. S. Narayan, *Appl. Phys. Lett.* **2008**, *92*, 093301.
[50] W. Tress, K. Leo, M. Riede, *Adv. Funct. Mater.* **2011**, *21*, 2140.
[51] A. Wagenpfahl, D. Rauh, M. Binder, C. Deibel, V. Dyakonov, *Phys. Rev. B* **2010**, *82*, 115306.
[52] H. Hoppe, M. Niggemann, C. Winder, J. Kraut, R. Hiesgen, A. Hinsch, D. Meissner, N. S. Sariciftci, *Adv. Funct. Mater.* **2004**, *14*, 1005.
[53] B. C. Thompson, J. M. J. Fréchet, *Angew. Chem. Int. Ed. Engl.* **2008**, *47*, 58.
[54] K. Vandewal, K. Tvingstedt, A. Gadisa, O. Inganäs, J. V Manca, *Nat. Mater.* **2009**, *8*, 904.
[55] K. Vandewal, A. Gadisa, W. D. Oosterbaan, S. Bertho, F. Banishoeib, I. Van Severen, L. Lutsen, T. J. Cleij, D. Vanderzande, J. V. Manca, *Adv. Funct. Mater.* **2008**, *18*, 2064.
[56] J. Rivnay, S. C. B. Mannsfeld, C. E. Miller, A. Salleo, M. F. Toney, *Chem. Rev.* **2012**, *112*, 5488.
[57] D. M. DeLongchamp, R. J. Kline, A. Herzing, *Energy Environ. Sci.* **2012**, *5*, 5980.